

On the solution of incompressible two-phase flow by a p-version discontinuous Galerkin method

Y. Epshteyn[‡] and B. Rivière^{*,†}

Department of Mathematics, University of Pittsburgh, 301 Thackeray, Pittsburgh, PA 15260, U.S.A.

SUMMARY

This paper presents a fully implicit scheme for approximating two-phase flow in heterogeneous porous media. The primary unknowns are the wetting phase pressure and non-wetting phase saturation. At each time step, a Jacobian matrix is computed. Convergence of the scheme is shown via increase of the polynomial degree. No slope limiters are needed. Copyright © 2005 John Wiley & Sons, Ltd.

KEY WORDS: fully-implicit pressure-saturation formulation; Newton–Raphson; non-symmetric and symmetric interior penalty Galerkin; high order polynomials

1. INTRODUCTION

The saturations of a wetting phase (s_w) and non-wetting phase (s_n) in incompressible two-phase flow in $\Omega \subset \mathbb{R}^2$ are characterized by the transport equation

$$\frac{\partial}{\partial t}(\phi s_\alpha) + \nabla \cdot \mathbf{u}_\alpha = q_\alpha, \quad \alpha = w, n \quad (1)$$

where $\mathbf{u}_\alpha = -\lambda_\alpha \mathbf{K} \nabla p_\alpha$ is the Darcy phase velocity, proportional to the gradient of the phase pressure p_α . The other coefficients in the model are: ϕ the porosity, q_α a source term, λ_α the phase mobility and \mathbf{K} the permeability of the porous medium. The difference between the phase pressures is the capillary pressure $p_c = p_n - p_w$ and we also assume that the sum of the phase saturations is equal to one. The boundary of Ω is divided into three disjoint parts

*Correspondence to: B. Rivière, Department of Mathematics, University of Pittsburgh, 301 Thackeray, Pittsburgh, PA 15260, U.S.A.

†E-mail: riviere@math.pitt.edu

‡E-mail: yee1@math.pitt.edu

Contract/grant sponsor: University of Pittsburgh; contract/grant number: 2004-39742

Received 3 June 2005

Revised 7 October 2005

Accepted 28 October 2005

Copyright © 2005 John Wiley & Sons, Ltd.

$\partial\Omega = \Gamma_0 \cup \Gamma_1 \cup \Gamma_2$, representing the inflow, outflow and no flow boundary, respectively, where we assume the following boundary conditions:

$$p_w = p_{\text{dir}} \quad \text{on } \Gamma_0 \cup \Gamma_1 \quad (2)$$

$$s_n = s_{\text{dir}} \quad \text{on } \Gamma_0 \quad (3)$$

$$\lambda_n \mathbf{K} \nabla p_c \cdot \mathbf{n} = 0 \quad \text{on } \Gamma_1 \quad (4)$$

$$\mathbf{u}_w \cdot \mathbf{n} = \mathbf{u}_n \cdot \mathbf{n} = 0 \quad \text{on } \Gamma_2 \quad (5)$$

The vector \mathbf{n} denotes the unit vector outward to the boundary.

Because of incompressibility, we can rewrite (1) into a pressure-saturation formulation [1], in which the primary variables are the wetting phase pressure and non-wetting phase saturation

$$-\nabla \cdot (\lambda_w + \lambda_n) \mathbf{K} \nabla p_w - \nabla \cdot \lambda_n \mathbf{K} \nabla p_c = q_w + q_n \quad (6)$$

$$-\frac{\partial}{\partial t}(\phi s_n) + \nabla \cdot \mathbf{u}_w = q_w \quad (7)$$

discontinuous finite element methods of high order that would handle heterogeneous permeability fields. Discontinuous Galerkin methods are well-suited for flow and transport problems in porous media because of their local mass conservation property and their flexibility [2]. The non-symmetric interior penalty Galerkin (NIPG) and symmetric interior penalty Galerkin (SIPG) methods have been successfully applied to flow and transport problem [3–6]. There is little work in the literature on DG applied to two-phase flow: in Reference [7], mixed finite elements are used with the combination of DG for the convective term. In References [8, 9], the NIPG method is applied to a sequential pressure-saturation formulation.

However, for convection-dominated problems, slope limiters [10, 11] are needed to prevent unstable overshoot and undershoot due to the high order of polynomial. Unfortunately, it is very complicated to design effective slope limiters for three-dimensional unstructured meshes and there is no analysis available in two or three dimensions.

In our proposed method, the coupled non-linear equations are solved by a Newton–Raphson method and one of the attractive features is that no slope limiters are used. Both symmetric and non-symmetric formulations are presented in Section 2. Section 3 presents the numerical experiments. Some conclusions follow.

2. FULLY IMPLICIT SCHEME

We now discretize the coupled equations (6) and (7) by a discontinuous Galerkin method in space. For that, we first introduce a quasi-uniform mesh $\mathcal{E}_h = \{E\}$ of Ω that consists of quadrilaterals. For any positive integer k , the discrete space is defined below

$$V_k = \{v \in L^2(\Omega) : v|_E \in \mathbb{P}_k(E) \quad \forall E \in \mathcal{E}_h\}$$

where $\mathbb{P}_k(E)$ is the set of polynomials of total degree k over E . Different orders are chosen for pressure and saturation and we denote by k_p (resp. k_s) the polynomial order for the pressure (resp. saturation). Let Γ_h denote the set of interior edges of \mathcal{E}_h . To each edge $e = \partial E_i \cup \partial E_j$ with $i > j$, we associate a unit normal vector \mathbf{n}_e from E_i to E_j that uniquely defines the jump of $v \in V_k$ as $[v] = v|_{E_i} - v|_{E_j}$. We also define the average of v by $\{v\} = 0.5(v|_{E_i} + v|_{E_j})$. For an edge e that belongs to the boundary $\partial\Omega$, the jump and average of v are defined to be the trace of v . For the time discretization, the backward Euler method is used. The time interval $(0, T)$ is divided into N subintervals of length $\Delta t = T/N$. Finally, we denote by $(\cdot, \cdot)_E$ the L^2 inner-product over the element E and by $\langle \cdot, \cdot \rangle_e$ the L^2 inner-product over the edge e .

The scheme is then: for $i = 1, \dots, N$ find $(p_w^i, s_n^i) \in V_{k_p} \times V_{k_s}$ satisfying

Pressure equation:

$$\begin{aligned} & \sum_{E \in \mathcal{E}_h} ((\lambda_w^i + \lambda_n^i) \mathbf{K} \nabla p_w^i + \lambda_n^i \mathbf{K} \nabla p_c^i, \nabla v)_E - \sum_{e \in \Gamma_h \cup \Gamma_0 \cup \Gamma_1} \langle \{(\lambda_w^i + \lambda_n^i) \mathbf{K} \nabla p_w^i \cdot \mathbf{n}_e\}, [v] \rangle_e \\ & - \sum_{e \in \Gamma_h \cup \Gamma_0} \langle \{\lambda_n^i \mathbf{K} \nabla p_c^i \cdot \mathbf{n}_e\}, [v] \rangle_e + \varepsilon \sum_{e \in \Gamma_h \cup \Gamma_0 \cup \Gamma_1} \langle \{(\lambda_w^i + \lambda_n^i) \mathbf{K} \nabla v \cdot \mathbf{n}_e\}, [p_w^i] \rangle_e \\ & + \varepsilon \sum_{e \in \Gamma_h \cup \Gamma_0} \langle \{\lambda_n^i \mathbf{K} \nabla v \cdot \mathbf{n}_e\}, [p_c^i] \rangle_e + \sum_{e \in \Gamma_h \cup \Gamma_0 \cup \Gamma_1} \frac{\sigma}{|e|} \langle [p_w^i], [v] \rangle_e + \sum_{e \in \Gamma_h \cup \Gamma_0} \frac{\sigma}{|e|} \langle [p_c^i], [v] \rangle_e \\ & = \sum_{E \in \mathcal{E}_h} (q_w^i + q_n^i, v)_E + \varepsilon \sum_{e \in \Gamma_0 \cup \Gamma_1} \langle (\lambda_w^i + \lambda_n^i) \mathbf{K} \nabla v \cdot \mathbf{n}_e, p_{dir} \rangle_e \\ & + \varepsilon \sum_{e \in \Gamma_0} \langle \lambda_n^i \mathbf{K} \nabla v \cdot \mathbf{n}_e, p_c(s_{dir}) \rangle_e + \sum_{e \in \Gamma_0 \cup \Gamma_1} \frac{\sigma}{|e|} \langle p_{dir}, v \rangle_e \\ & + \sum_{e \in \Gamma_0} \frac{\sigma}{|e|} \langle p_c(s_{dir}), v \rangle_e \quad \forall v \in V_{k_p} \end{aligned}$$

Saturation equation:

$$\begin{aligned} & - \frac{1}{\Delta t} (\phi s_n^i, z) + \sum_{E \in \mathcal{E}_h} (\lambda_w^i \mathbf{K} \nabla p_w^i, \nabla z)_E - \sum_{e \in \Gamma_h \cup \Gamma_0 \cup \Gamma_1} \langle \{\lambda_w^i \mathbf{K} \nabla p_w^i \cdot \mathbf{n}_e\}, [z] \rangle_e \\ & + \varepsilon \sum_{e \in \Gamma_h \cup \Gamma_0 \cup \Gamma_1} \langle \{\lambda_w^i \mathbf{K} \nabla z \cdot \mathbf{n}_e\}, p_w^i \rangle_e + \sum_{e \in \Gamma_h \cup \Gamma_0 \cup \Gamma_1} \frac{\sigma}{|e|} \langle [p_w^i], [z] \rangle_e = (q_w^i, z) - \frac{1}{\Delta t} (\phi s_n^{i-1}, z) \\ & + \varepsilon \sum_{e \in \Gamma_0 \cup \Gamma_1} \langle \lambda_w^i \mathbf{K} \nabla z \cdot \mathbf{n}_e, p_{dir} \rangle_e + \sum_{e \in \Gamma_0 \cup \Gamma_1} \frac{\sigma}{|e|} \langle p_{dir}, z \rangle_e \quad \forall z \in V_{k_s} \end{aligned}$$

The resulting scheme for the choice $\varepsilon = 1$ is referred as the NIPG method whereas the choice $\varepsilon = -1$ yields the SIPG method. The parameter σ is a positive constant in a stabilizing term that penalizes the jump of the wetting phase pressure and the jump in the capillary pressure. The coefficients λ_w^i, λ_n^i and p_c^i depend on the non-wetting phase saturation in a non-linear

fashion. Using the Brooks–Corey [12] model, we have

$$\lambda_w^i = \frac{(1 - s_n^i)^{11/3}}{\mu_w}, \quad \lambda_n = \frac{(s_n^i)^2(1 - (1 - s_n^i)^{5/3})}{\mu_n}, \quad p_c^i = p_d(1 - s_n^i)^{-1/3}$$

where μ_w and μ_n are the phase viscosities and p_d a constant entry pressure. The equations above are non-linear in p_w^i and s_n^i ; thus a Newton–Raphson method is utilized and a Jacobian matrix is computed at each time step. For convergence of the Newton–Raphson algorithm, the choice of initial pressure and saturation is crucial, in particular for the first time step. On one hand, the initial saturation is easily chosen to be equal to $s_n^0 = 1.0 - s_{wr}$, where s_{wr} is the residual wetting phase saturation, i.e. the amount of wetting phase always present in the medium. On the other hand, the initial pressure p_w^0 is the solution of the linear problem

$$\begin{aligned} & \sum_{E \in \mathcal{E}_h} ((\lambda_w^0 + \lambda_n^0) \mathbf{K} \nabla p_w^0, \nabla v)_E - \sum_{e \in \Gamma_h \cup \Gamma_0 \cup \Gamma_1} \langle \{(\lambda_w^0 + \lambda_n^0) \mathbf{K} \nabla p_w^0 \cdot \mathbf{n}_e\}, [v] \rangle_e \\ & + \varepsilon \sum_{e \in \Gamma_h \cup \Gamma_0 \cup \Gamma_1} \langle \{(\lambda_w^0 + \lambda_n^0) \mathbf{K} \nabla v \cdot \mathbf{n}_e\}, [p_w^0] \rangle_e + \sum_{e \in \Gamma_h \cup \Gamma_0 \cup \Gamma_1} \frac{\sigma}{|e|} \langle [p_w^0], [v] \rangle_e \\ & = \sum_{E \in \mathcal{E}_h} (q_w^0 + q_n^0, v)_E + \varepsilon \sum_{e \in \Gamma_0 \cup \Gamma_1} \langle (\lambda_w^0 + \lambda_n^0) \mathbf{K} \nabla v \cdot \mathbf{n}_e, p_{dir} \rangle_e + \sum_{e \in \Gamma_0 \cup \Gamma_1} \frac{\sigma}{|e|} \langle p_{dir}, v \rangle_e \\ & - \sum_{E \in \mathcal{E}_h} (\lambda_n^0 \mathbf{K} \nabla p_c^0, \nabla v)_E + \sum_{e \in \Gamma_h \cup \Gamma_0} \langle \{\lambda_n^0 \mathbf{K} \nabla p_c^0 \cdot \mathbf{n}_e\}, [v] \rangle_e \\ & - \varepsilon \sum_{e \in \Gamma_h \cup \Gamma_0} \langle \{\lambda_n^0 \mathbf{K} \nabla v \cdot \mathbf{n}_e\}, [p_c^0] \rangle_e - \sum_{e \in \Gamma_h \cup \Gamma_0} \frac{\sigma}{|e|} \langle [p_c^0], [v] \rangle_e \\ & + \varepsilon \sum_{e \in \Gamma_0} \langle \lambda_n^0 \mathbf{K} \nabla v \cdot \mathbf{n}_e, p_c(s_{dir}) \rangle_e + \sum_{e \in \Gamma_0} \frac{\sigma}{|e|} \langle p_c(s_{dir}), v \rangle_e \end{aligned}$$

For the other time steps, the initial Newton iterates are taken to be the approximate solutions at the previous time. In our numerical experiments, the Newton iterations converge when the residuals are less than 10^{-7} . In all simulations, the convergence of Newton’s method is fast; the first Newton step converges with 7 iterations, then the successive Newton steps converge with 4 iterations; and sometimes the last Newton step reaches convergence after 3 iterations.

3. NUMERICAL EXAMPLES

We consider a domain $(0, 100)^2$ with heterogeneous permeability $\mathbf{K} = k\mathbf{I}$ with $k = 5 \times 10^{-9} \text{m}^2$ in most of the domain except in an inclusion $\{37.5 \leq x \leq 100\} \times \{37.5 \leq y \leq 62.5\}$ where $k = 5 \times 10^{-13} \text{m}^2$ (see Figure 1). The domain has been subdivided into 64 rectangular elements. The wetting phase enters the domain through the left vertical boundary $\Gamma_0 = \{0\} \times (0, 100)$ with the Dirichlet value $s_{dir} = 0.85$. On Γ_0 , the pressure is $p_w = 3 \times 10^6 \text{Pa}$. On the outflow boundary $\Gamma_1 = \{100\} \times (0, 100)$, the pressure is set to $p_w = 10^6 \text{Pa}$. The residual wetting phase saturation is $s_{wr} = 0.2$. The penalty parameter is fixed to $\sigma = 0.1$. The

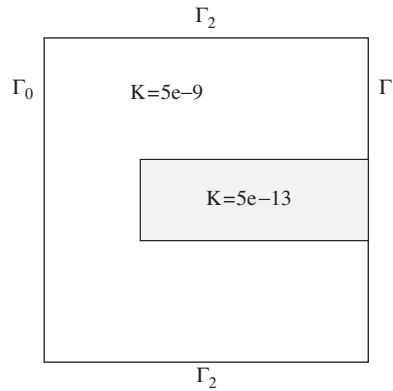


Figure 1. Heterogeneous permeability field.

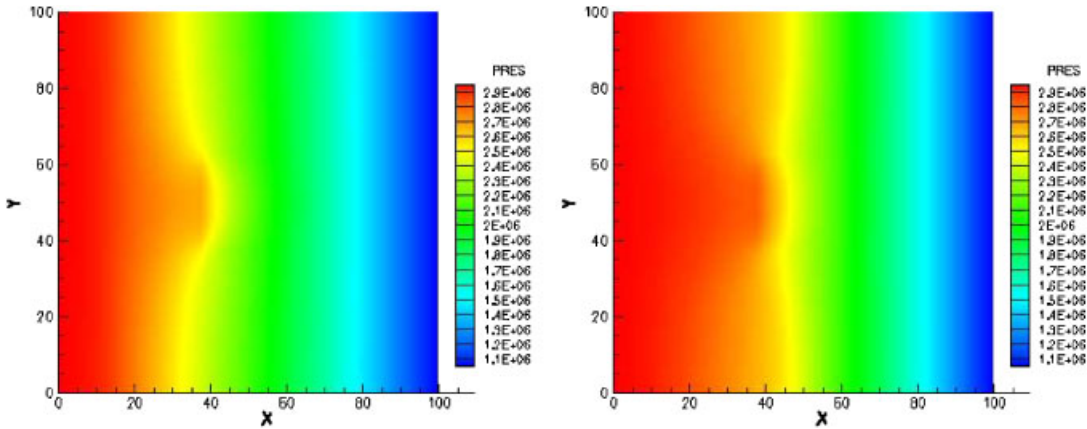


Figure 2. Contours of pressure at 200 (left) and 600 (right) days: $k_p = 4$.

other physical coefficients are $\phi = 0.2, \mu_w = 0.001, \mu_n = 0.01$ and $p_d = 1000$ Pa. Unless specified otherwise, the basis functions for the discrete space V_k are the monomial functions $x^i y^j$ for $i + j \leq k$.

First, we show the evolution of the pressure from 200 days to 600 days in Figure 2. In this case, $k_p = 4, k_s = 2$ and the NIPG method is used (i.e $\varepsilon = 1$). We also show the contours of the wetting phase saturation at 600 and 900 days in Figures 3 and 4. Both pressure and saturation contours take into account the heterogeneity of the permeability field; the low permeability region acts as an impermeable zone where the wetting phase saturation does not penetrate.

Second, we show numerical convergence of the NIPG scheme by increasing the polynomial order. Figure 5 shows the contour of the pressure at 600 days and the saturation at 900 days for the case where the pressure is approximated by piecewise cubics and the saturation by piecewise linears. The wetting phase is flooding the domain as if the permeability was uniform.

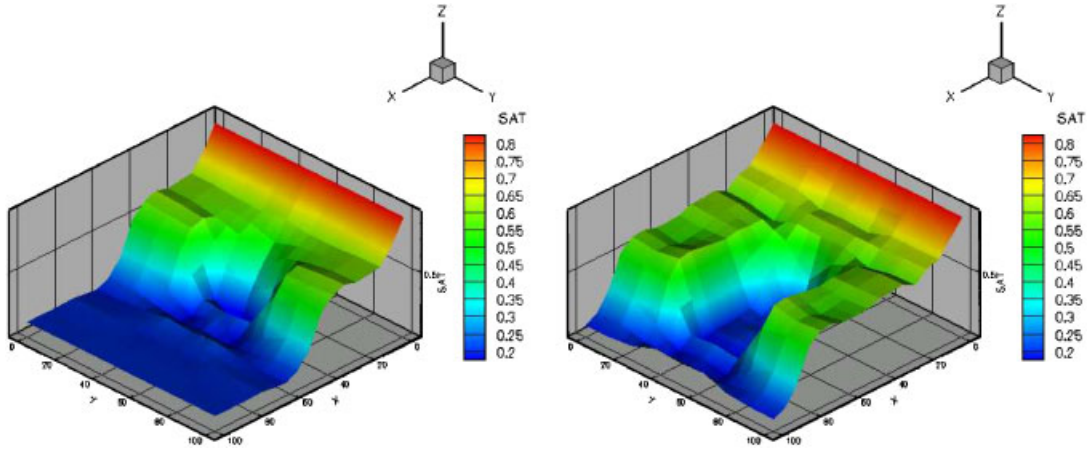


Figure 3. Three-dimensional contours of saturation at 600 (left) and 900 (right) days: $k_s = 2$.

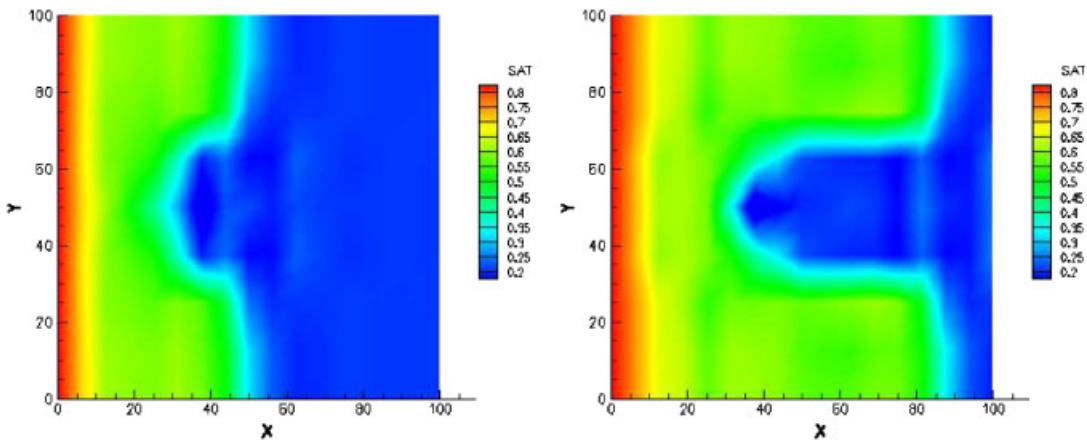


Figure 4. Contours of saturation at 600 (left) and 900 (right) days ($k_s = 2$).

Then, we increase both polynomial degrees by using quartic polynomials for pressure and quadratic polynomials for saturation (Figure 6). The contour of the pressure is very slightly modified, but there is a significant change in the saturation contour. By further increasing the polynomial degree ($k_p = 5$ and $k_s = 3$), a more accurate approximate solution is obtained (Figure 7). We then continue to increase the polynomial degrees k_p, k_s . To better see the convergence, we plot the contour of the wetting phase pressure and saturation along the line $\mathcal{L} = (0, 100) \times \{50\}$ in Figure 8. Here, k_p varies from 3 to 7 and k_s varies from 1 to 5. The pressure contours do not vary much for higher degree, but the saturation front is sharper as

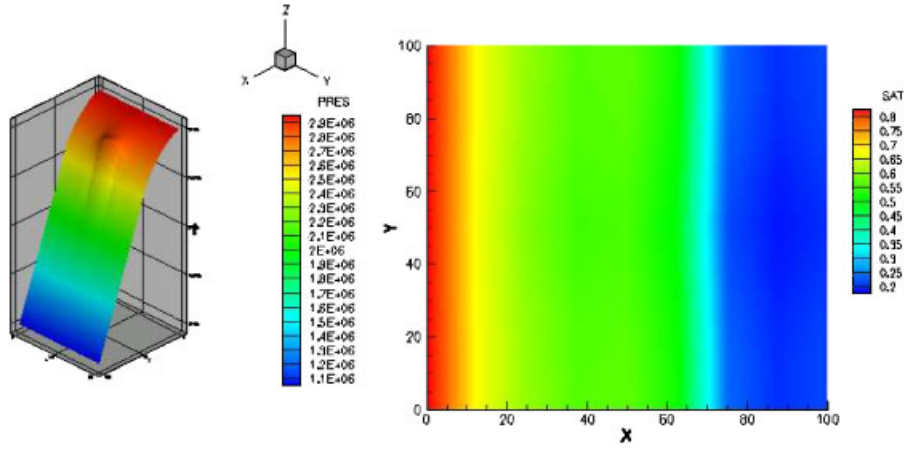


Figure 5. Pressure contour $k_p = 3$ at 600 days (left) and saturation contours $k_s = 1$ at 900 days (right).

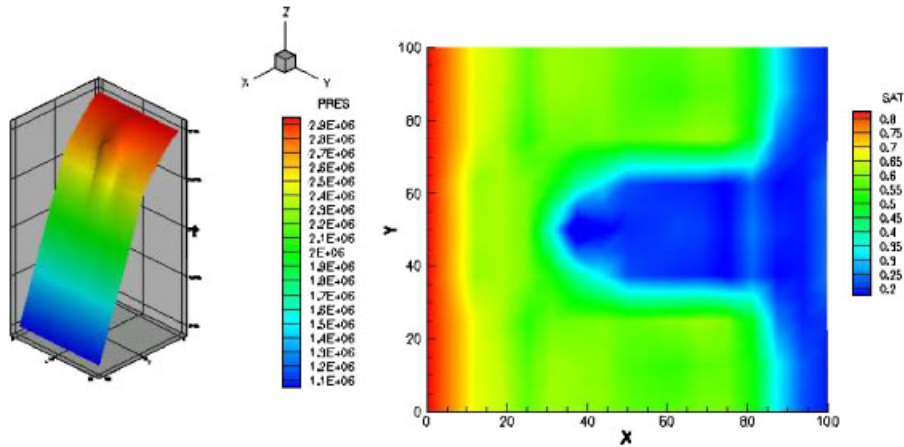


Figure 6. Pressure contour $k_p = 4$ at 600 days (left) and saturation contours $k_s = 2$ at 900 days (right).

k_s increases. Thus, we show that the p-version of this scheme converges numerically, even on a very coarse mesh.

Next, we compare the symmetric and non-symmetric formulations for the case where the pressure is approximated by quartics and saturation by quadratics. Figure 9 shows the pressure contours at 600 days. The contour of the saturation along the line \mathcal{L} is shown in Figure 10 at 300 and 900 days. We observe that both schemes yield the same approximate solutions. The contours coincide with each other. This is also true for the other choices of polynomial degrees. Figure 10 also shows some small oscillations at 900 days. These oscillations decrease

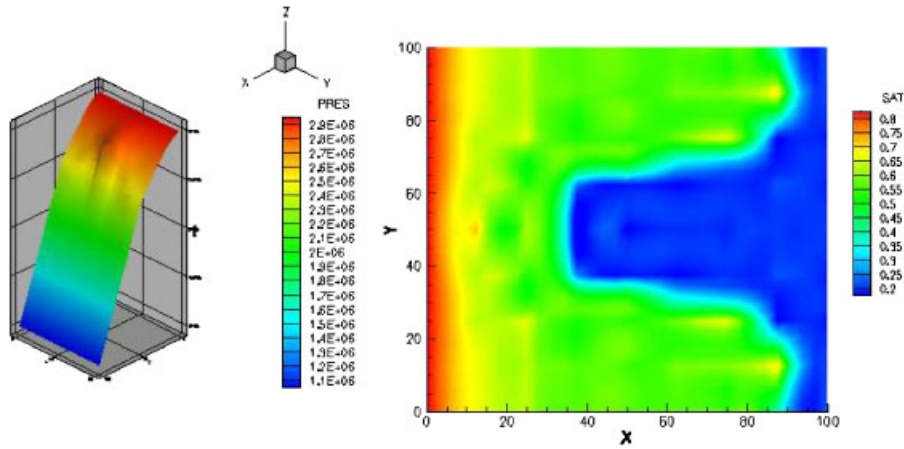


Figure 7. Pressure contour $k_p = 5$ at 600 days (left) and saturation contours $k_s = 3$ at 900 days (right).

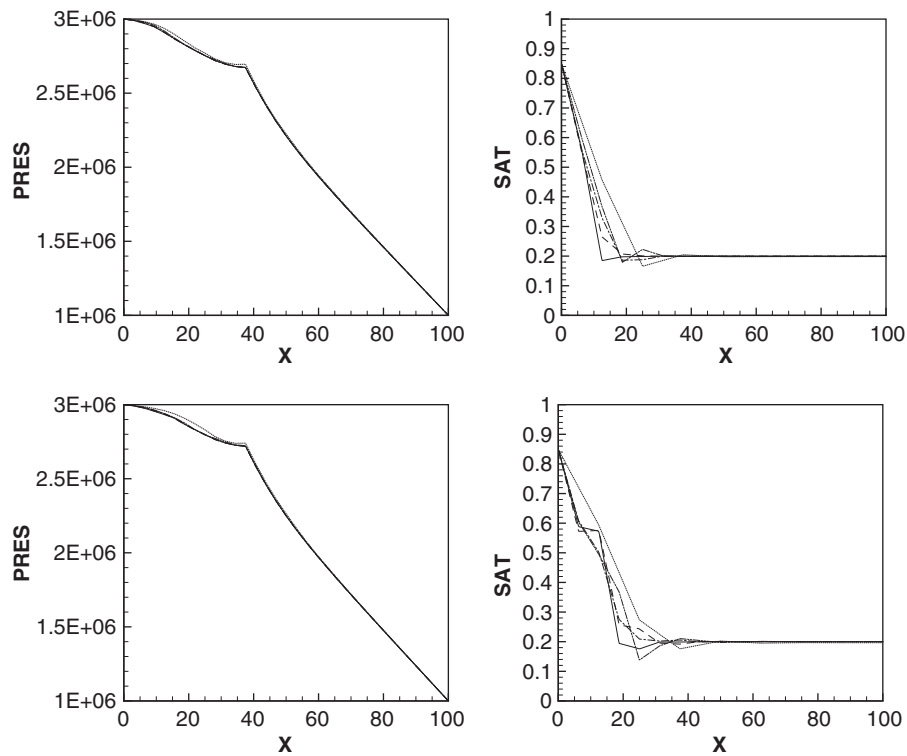


Figure 8. Pressure (left) and saturation (right) contour along \mathcal{L} at 200 days (top) and 300 days (bottom): dotted line $k_p = 3, k_s = 1$, dash-dot-dotted line $k_p = 4, k_s = 2$, dash-dot line $k_p = 5, k_s = 3$, dashed line $k_p = 6, k_s = 4$, solid line $k_p = 7, k_s = 5$.

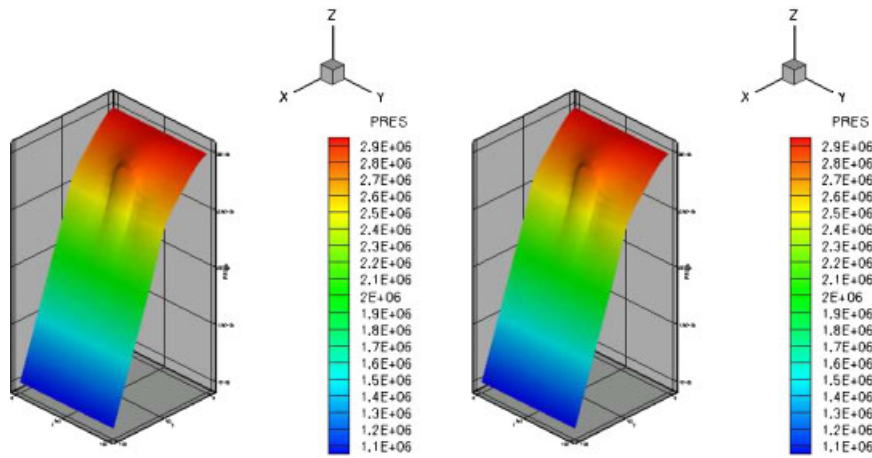


Figure 9. SIPG (left) and NIPG (right) pressure contours at 600 days: $k_p = 4$.

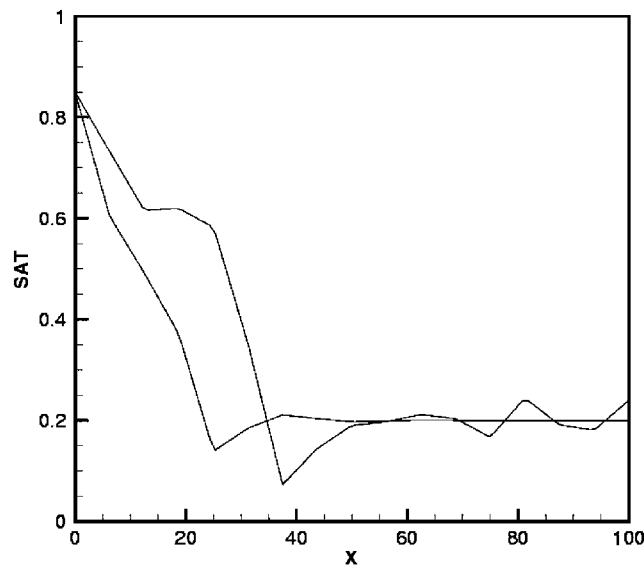


Figure 10. Comparison between NIPG and SIPG saturation at 300 and 900 days: $k_s = 2$.

significantly with refining the mesh and we think that these oscillations are the result of a too coarse mesh and a long simulation time.

Finally, we study the effects of different basis functions of V_k on the coarse mesh. We compare monomial basis functions with Legendre polynomials. In Figures 11 and 12, the pressure and saturation contours along the line \mathcal{L} are shown. There is no noticeable difference

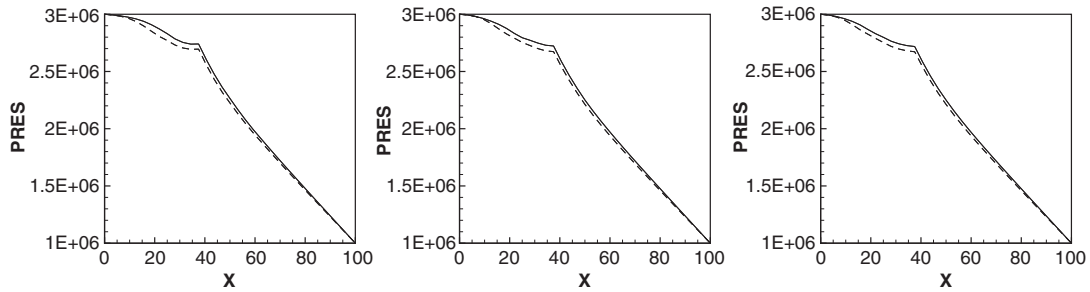


Figure 11. NIPG pressure at 200 days (dashed line) and 300 days (solid line): comparison between monomial and Legendre basis functions: $k_p = 3$ (left), $k_p = 4$ (centre) and $k_p = 5$ (right).

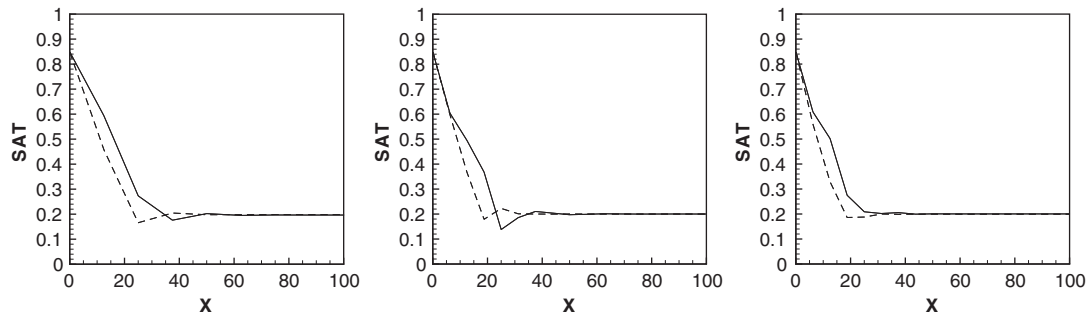


Figure 12. NIPG saturation at 200 days (dashed line) and 300 days (solid line): comparison between monomial and Legendre basis functions: $k_s = 1$ (left), $k_s = 2$ (centre) and $k_s = 3$ (right).

between the two simulations. The two types of basis yield comparable numbers of Newton iterations for convergence, and also similar simulation times.

4. CONCLUSIONS

This paper presents the p-convergence of a class of discontinuous finite element methods for a fully-implicit formulation of the two-phase flow problem in heterogeneous medium. At each time step, the Newton iterations converge very quickly. One of the surprising benefits of solving fully coupled equations is that no slope limiters are needed to stabilize the high order approximation. Comparisons between SIPG and NIPG show that they produce the same numerical solutions.

REFERENCES

1. Helmig R. *Multiphase Flow and Transport Processes in the Subsurface*. Springer: Berlin, 1997.
2. Cockburn B, Karniadakis GE, Shu C-W (eds). *First International Symposium on Discontinuous Galerkin Methods*. Lecture Notes in Computational Science and Engineering, 2000.

3. Rivière B, Wheeler MF. Non conforming methods for transport with nonlinear reaction. *Fluid Flow and Transport in Porous Media: Mathematical and Numerical Treatment* 2002; **295**:421–430.
4. Rivière B, Wheeler MF. Discontinuous Galerkin methods for flow and transport problems in porous media. *Communications in Numerical Methods in Engineering* 2002; **18**:63–68.
5. Sun S, Rivière B, Wheeler MF. A combined mixed finite element and discontinuous Galerkin method for miscible displacement problem in porous media. *Recent Progress in Computational and Applied PDEs* 2002; 323–351.
6. Bastian P. Higher order discontinuous Galerkin methods for flow and transport in porous media. *Challenges in Scientific Computing—CISC 2002* 2003; **35**:1–22.
7. Nayagum D, Schäfer G, Mosé R. Modelling two-phase incompressible flow in porous media using mixed hybrid and discontinuous finite elements. *Computational Geosciences* 2004; **8**(1):49–73.
8. Rivière B. Numerical study of a discontinuous Galerkin method for incompressible two-phase flow. *ECCOMAS Proceedings*, 2004.
9. Bastian P, Rivière B. Discontinuous Galerkin methods for two-phase flow in porous media. *University of Heidelberg Technical Report 2004-28*, 2004.
10. Chavent G, Jaffré J. Mathematical models and finite elements for reservoir simulation. *Studies in Mathematics and its Applications* 1986.
11. Cockburn B, Shu CW. TVB Runge–Kutta local projection discontinuous Galerkin finite element method for conservative laws II: general framework. *Mathematics of Computation* 1989; **52**:411–435.
12. Brooks R, Corey A. Hydraulic properties of porous media. *Colorado State University Hydrology Paper* 3, 1979.